IL NUOVO CIMENTO **45 C** (2022) 162
DOI 10.1393/ncc/i2022-22162-0

COMMUNICATIONS: SIF Congress 2021

Scenario modelling for the Divertor Tokamak Test facility

I. CASIRAGHI[2][3], P. MANTICA[3], R. AMBROSINO[4][5][1], L. AUCONE[2][3], B. BAIOCCHI[3], L. BALBINOT[6][7], A. CASTALDO[5], J. CITRIN[8][9], L. FRASSINETTI[10], P. INNOCENTE[7], F. KOECHL[11], A. MARIANI[2][3], P. AGOSTINETTI[7], S. CECCUZZI[12][1], L. FIGINI[3], G. GRANUCCI[3] and M. VALISA[7]

([1]) *DTT S.C. a r.l. - Frascati, Italy*
([2]) *Dipartimento di Fisica, Università degli Studi di Milano-Bicocca - Milano, Italy*
([3]) *Istituto per la Scienza e Tecnologia dei Plasmi, CNR - Milano, Italy*
([4]) *Università degli Studi di Napoli Federico II - Napoli, Italy*
([5]) *Consorzio CREATE - Napoli, Italy*
([6]) *Università degli Studi di Padova - Padova, Italy*
([7]) *Consorzio RFX - Padova, Italy*
([8]) *DIFFER, Dutch Institute for Fundamental Energy Research Eindhoven, The Netherlands*
([9]) *Science and Technology of Nuclear Fusion Group, Eindhoven University of Technology Eindhoven, The Netherlands*
([10]) *Fusion Plasma Physics, ECSS, KTH Royal Institute of Technology - Stockholm, Sweden*
([11]) *CCFE, Culham Science Centre - Abingdon, UK*
([12]) *ENEA C.R. Frascati - Frascati, Italy*

received 31 January 2022

Summary. — The scenario integrated modelling is a top priority work during the design of a new tokamak, as the Divertor Tokamak Test facility (DTT) under construction at the ENEA Research Center in Frascati. The first simulations of the main baseline scenarios contributed to the optimization of the DTT project, particularly with regard to the machine size and heating systems, besides serving as reference for diagnostics design. In this paper we report the first simulations of the full power baseline scenario in the final configuration of the machine and heating mix.

1. – Introduction

In the European Roadmap towards thermonuclear fusion power production, studying the controlled exhaust of energy and particles from a fusion reactor is a top priority research item. This is the main goal of the Divertor Tokamak Test facility (DTT), a new D-shaped superconducting tokamak ($R = 2.19\,\mathrm{m}$, $a = 0.70\,\mathrm{m}$, W first wall and divertor,

vacuum toroidal field $B_T \leq 5.85\,\mathrm{T}$, plasma current $I_p \leq 5.5\,\mathrm{MA}$, pulse length $\leq$100 s, auxiliary heating $\leq$45 MW), whose construction is ongoing in Frascati.

In support of the device design, it is a key priority to achieve multi-channel simulations of DTT scenarios based on state-of-the-art first-principle quasi-linear transport models. This integrated modelling, started less than 3 years ago, is widely described in [1]. This work led to the decision of a machine enlargement (in the previous configuration $R = 2.14\,\mathrm{m}$ and $a = 0.65\,\mathrm{m}$) with consequent auxiliary heating system upgrades.

This paper reports first results of integrated modelling of the full power baseline scenario for the DTT final configuration.

2. – The integrated modelling

These integrated simulations solve the transport equations for heat, particle, and momentum using a quasi-linear transport model in a self-consistent magnetic equilibrium and with heating profiles also calculated consistently. Steady-state radial profiles of main ion and electron temperatures and densities, impurity densities, rotation, current density, and other physical quantities were predicted for the full power (FP) reference scenario with the Single Null (SN) magnetic configuration with positive triangularity during the flat-top phase.

2˙1. *Full power reference scenario heating.* – DTT will be equipped with three auxiliary heating systems in the FP reference scenario ($B_T = 5.85\,\mathrm{T}$, $I_p = 5.5\,\mathrm{MA}$), to supply around 45 MW to the plasma.

Particularly, it will include 32 gyrotrons at 170 GHz gathered in 4 ECRH clusters with an installed power of 1 MW from each gyrotron (∼0.9 MW to the plasma per gyrotron), 4 RF two-strap antennas operating at 60–90 MHz assembled in 2 ICRH modules with an installed power of 2 MW from each antennas (∼1.5 MW to the plasma per antenna), and a negative-ion–based NBI system composed of one injector at 510 keV providing a power of ∼10 MW to the plasma. In this work, the RF antennas operate at a frequency of 90 MHz, using hydrogen as minority species with a concentration of 5%.

2˙2. *Simulation settings.* – The simulation of the FP scenario was performed using both the ASTRA [2] transport solver and the JINTRAC [3] suite of codes within an iterative ASTRAJINTRAC scheme to obtain a high complexity run. Indeed, this mixed method allow us to have a much faster ASTRA run combined with advantageous contributions of the JINTRAC codes (especially, impurity and heating codes). Particularly, the JINTRAC runs employ interpretative T_e, T_i, and n_e profiles taken from the previous ASTRA step, while the ASTRA runs uses prescribed profiles of impurities, radiation, and heatings provided by the previous JINTRAC step.

The heat and particle transport equations are solved from the plasma centre up to the top of the pedestal. Particularly, the neoclassical transport is calculated by the NCLASS [4] model, while the turbulent transport is calculated by TGLF SAT2 [5], which is a gyrofluid electromagnetic quasi-linear model with shaped flux surfaces. The toroidal rotation is predicted using a theory-driven empirical model [6-8], keeping fixed the Prandtl number $\chi_\varphi/\chi_i = 0.7$ and adjusting the pinch number RV_φ/χ_i using the parameter dependences given in [7, 8] (more details in [1]).

The MHD equilibrium is self-consistently recalculated by the equilibrium solver ESCO in the JINTRAC steps and by the SPIDER [9] code in the ASTRA steps. The plasma boundary is kept fixed to that of the starting reference DTT plasma equilibria provided by the free boundary CREATE-NL [10] solver.

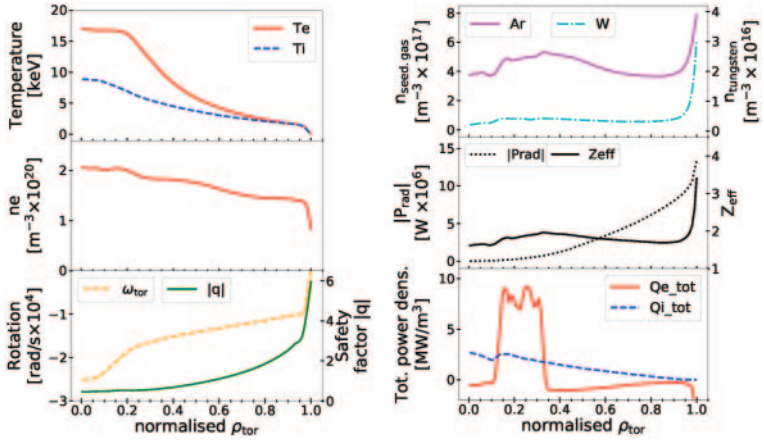

Fig. 1. – On the left, radial profiles of T_e, T_i, n_e, $\omega_{\rm tor}$, and $|q|$ in the FP SN PT scenario calculated by TGLF. On the right, radial profiles of seeding gas density, tungsten density, radiative power, effective charge, $Q_{e,\rm tot}$, and $Q_{i,\rm tot}$.

Two impurities are included in the run: argon as seeding gas, used to enlarge the edge radiative dissipation decreasing the divertor power load, and tungsten, coming from the divertor and the first wall. Radiation and impurity densities are calculated by the SANCO [11] code during the JINTRAC stages, treating the ionisation states separately and setting an impurity density ratio $n_{\rm W}/n_{\rm Ar} = 0.01$. Then, these profiles are simply taken from JINTRAC and used in ASTRA, which presently is not equipped with an impurity code.

In the pedestal region, the kinetic profiles are fixed to the values calculated previously by an Europed [12] run using the EPED [13] model. In the Europed simulation, $\beta_{\rm pol} = 0.55$, $T_{\rm sep} = 130\,{\rm eV}$, $n_{e,\rm ped} = 1.4\times10^{20}/\,{\rm m}^3$, and a relative shift between n_e and T_e tuned to obtain $n_{e,\rm sep} \approx 8\times10^{19}/\,{\rm m}^3$, and argon as impurity with $Z_{\rm eff} = 1.8$ were set. The $n_{e,\rm ped}$ value has been tuned to reach the Greenwald fraction target value of $\langle n_e\rangle/n_G{\sim}0.45$ (where n_G is the Greenwald density as defined in [14]).

Heating and current drive are computed several times during the JINTRAC steps by specific codes and then these profiles are fixed to the JINTRAC calculations during the ASTRA steps. The PENCIL [15] code and the PION [16,17] code calculate the NBI and the ICRH power deposition respectively. The synergy effects between NBI and ICRH systems result non-negligible. Currently, the ECRH power density calculations by the GRAY [18] code are being included in the integrated modelling with poloidal and toroidal beam angles tuned to have an EC current drive which moves the $q = 1$ point inward to reach a more stable condition.

Furthermore, in the JINTRAC steps of the simulation, the total neutron number is calculated in the JETTO simulations as the sum of neutrons produced by the fusion reactions between: two thermal nuclei, a thermal nucleus and a fast nucleus of the NBI beam, a thermal nucleus and a fast nucleus of the ICRH minority species.

So far, the modelling does not include ELMs (Edge Localised Modes) and sawteeth, hence the profiles presented here depict the condition of saturated recovery after a sawtooth crash.

Thanks to these simulation settings, the edge values of the integrated modelling presented here result compatible with conditions for the detachment.

2˙3. *Full power scenario results.* – The predicted radial profiles of electron temperature T_e, ion temperature T_i, electron density n_e, rotation $\omega_{\rm tor}$, safety factor q, argon density, tungsten density, radiative power $P_{\rm rad}$, effective charge $Z_{\rm eff}$, total electron power density $Q_{e,\rm tot}$, and total ion power density $Q_{i,\rm tot}$ are shown in fig. 1. The total power densities are calculated including the thermal exchange power between electrons and ions due to the collisional coupling. At the plasma centre, $T_{e,0} \approx 18.0\,\rm keV$, $T_{i,0} = 9\,\rm keV$, and $n_{e,0} = 2.05 \times 10^{20}/\,\rm m^3$ values are reached.

We notice that $T_e \gg T_i$ over almost all plasma radii. For $T_e/T_i > 1$, the threshold of the ion temperature gradient modes (ITGs) is low and TGLF predicts high ion stiffness, so T_i cannot increase in spite of the collisional power flowing from electrons to ions. A possible way to equilibrate more the two temperatures would be increasing the electron density to enhance the collisional coupling. However, due to the shallow dependence of the ITG threshold on $T_e/T_i > 1$ in this parameter region, this would result more in electron temperature reduction than in ion temperature growth. Furthermore, the n_e increase is limited by the ECRH cut-off.

We also note from fig. 1 that impurities do not significantly accumulate in the centre. The total neutron rate approximately equal to 10^{17} neutrons/s is compatible with the present design of neutron shields with a good safety margin.

3. – Conclusions

The steady-state simulation of the flat-top phase of the DTT full power baseline scenario with the recently finalised device configuration is now available.

* * *

This work has been carried out in the framework of the DTT design. The authors are very grateful to all colleagues involved in the DTT project for their essential contributions. The first author has worked under a PhD grant financed by ENEA.

REFERENCES

[1] Casiraghi I. *et al.*, *Nucl. Fusion*, **61** (2021) 116068.
[2] Pereverzev G. V. and Yushmanov P. N., *ASTRA automated system for transport analysis in a tokamak*, IPP Report 5/98 (Max-Planck-Institut für Plasmaphysik) 2002.
[3] Romanelli M. *et al.*, *Plasma Fusion Res.*, **9** (2014) 3403023.
[4] Houlberg W. A. *et al.*, *Phys. Plasmas*, **4** (1997) 3230.
[5] Staebler G. M. *et al.*, *Plasma Phys. Control. Fusion*, **63** (2021) 015013.
[6] Peeters A. G. *et al.*, *Nucl. Fusion*, **51** (2011) 094027.
[7] Peeters A. G., Angioni C. and Strintzi D., *Phys. Rev. Lett.*, **98** (2007) 265003.
[8] Peeters A. G. *et al.*, *Phys. Plasmas*, **16** (2009) 062311.
[9] Ivanov A. A., *32nd EPS Conf. Plasma Physics Terragona 29C (ECA)*, **5** (2005) 063.
[10] Albanese R., Ambrosino R. and Mattei M., *Fusion Eng. Des.*, **96-97** (2015) 664.
[11] Taroni L. *et al.*, *21st EPS Europhys. Conf. Abstr.*, **18B** (1994) 102.
[12] Saarelma S. *et al.*, *Plasma Phys. Control. Fusion*, **60** (2018) 014042.
[13] Snyder P. B. *et al.*, *Nucl. Fusion*, **51** (2011) 103016.
[14] Greenwald M., *Plasma Phys. Control. Fusion*, **44** (2002) R27.
[15] Challis C. D. *et al.*, *Nucl. Fusion*, **29** (1989) 563.
[16] Eriksson L.-G., Hellsten T. and Willen U., *Nucl. Fusion*, **33** (1993) 1037.
[17] Hellsten T. and Eriksson L.-G., *Nucl. Fusion*, **29** (1989) 2165.
[18] Farina D., *Fusion Sci. Technol.*, **52** (2007) 154.